Simulation of the cytoskeletal response of cells on grooved or patterned substrates

A. Vigliotti[¶], R.M. McMeeking[§] and V.S. Deshpande[¶1]

[¶]Department of Engineering, University of Cambridge, Cambridge CB2 1PZ, U.K.
[§]Mechanical Engineering and Materials Departments, University of California, Santa Barbara CA 93106, USA and School of Engineering, University of Aberdeen, King's College, Aberdeen AB24 3UE, U.K.

Abstract

We analyze the response of osteoblasts on grooved substrates via a model that accounts for the co-operative feedback between intracellular signaling, focal adhesion development and stress fiber contractility. The grooved substrate is modeled as a pattern of alternating strips on which the cell can adhere and strips on which adhesion is inhibited. The coupled modeling scheme is shown to capture some key experimental observations including: (i) the observation that osteoblasts orient themselves randomly on substrates with groove pitches less than about 150 nm but they align themselves with the direction of the grooves on substrates with larger pitches, and (ii) actin fibers bridge over the grooves on the substrates with groove pitches less than about 150 nm but form a network of fibers aligned with the ridges, with nearly no fibers across the grooves, for substrates with groove pitches greater than about 300 nm. Using the model, we demonstrate that the degree of bridging of the stress fibers across the grooves, and consequently the cell orientation, is governed by the diffusion of signaling proteins activated at the focal adhesion sites on the ridges. For large groove pitches the signaling proteins are dephosphorylated before they can reach the regions of the cell above the grooves and hence stress fibers cannot form in those parts of the cell. On the other hand, the stress fiber activation signal diffuses to a reasonably spatially homogenous level on substrates with small groove pitches and hence stable stress fibers develop across the grooves in these cases. The model thus rationalizes the responsiveness of osteoblasts to the topography of substrates based on the complex feedback involving focal adhesion formation on the ridges, the triggering of signaling pathways by these adhesions and the activation of stress fiber networks by these signals.

Keywords: *mechano-sensitivity, cell signaling, focal adhesions, actin/myosin contractility*.

[1] Author for correspondence (vsd@eng.cam.ac.uk)

1. Introduction

Cells are known to be very sensitive to their mechanical, chemical and topographical environments. For example mesenchymal stem cells (MSCs) sense and respond to the stiffness of the substrate they are cultured on and differentiate into bone cells when cultured on stiff substrates, but give rise to neuronal cells under identical conditions when soft substrates were used [1]. Similarly, endothelial cells sense stresses and display an increased proliferation rate in regions of high tractions [2]. The ability of MSCs to sense their chemical environment was shown by using ligand patterns [3] to limit the spreading of cells. Limiting spreading increases the tendency of MSCs to differentiate into fat cells in contrast to their tendency to become bone cells when allowed to spread. Building on these strategies, McMurray et al. [4] embossed substrates to pattern square-shaped pits 120 nm in size, arranged in a square lattice with a separation of 180 nm between the pits. They observed that MSCs cultured on the pitted substrates maintained an undifferentiated state for up to eight weeks, whereas cells on the control (planar) substrates rapidly differentiated into various cell types (mostly bone cells), thus demonstrating that the topography of the substrate too has a profound effect on the preservation of pluripotency.

The cell's cytoskeleton, which influences a broad range of cellular activities in a tension-dependent manner, interacts with the substrate through focal adhesions (FAs) — these multiprotein structures in turn transmit regulatory signals (among them, mechanical signals). For example, a tense cytoskeleton favors differentiation of MSCs into bone cells. The organization and signaling properties of the cytoskeleton can be engineered with nano-patterned substrates: these patterns define the positions, shapes and sizes of the focal adhesions and thereby control the responsiveness of cells to substrate topography. It is thought that similar mechanisms are also employed in-vivo to control proliferation and differentiation of cells. For example, natural bone ECM (extra-cellular matrix) is a highly organized nano-composite consisting of, among other things, molecules of type-I collagen. Collagen type-I forms fibrils with a interfibrillar spacing of 68 nm and 35 nm depth [5] and a number of studies [6-8] have demonstrated that mimicking such roughness in-vitro has beneficial effects on osteoblast proliferation. The role of the collagen fibrillar organization in controlling the arrangement of the actin cytoskeleton has sometimes been referred to as "contact guidance" [9-10]. In numerous situations [11] contact guidance prevails over mechanical cues such as cyclic stretching in governing the arrangement of the cytoskeleton, confirming the importance of the topographical environment of cells.

The response of cells to substrates with ordered textures has received considerable attention [12-15]. These studies indicate that cells are especially responsive to groove/ridge patterns on the substrate. Of particular note is the study of Lamers et al. [16] who created groove patterns (Fig. 1) that best mimic the in-vivo length scales of the collagen fibrillar network in natural bone ECM. Their study demonstrated that osteoblasts were responsive to substrates with groove pitches down to approximately 75 nm: at lower pitches the cytoskeletal network was random but with increasing groove pitch the actin filaments of the cytoskeleton increasingly aligned with the groove (or ridge direction). They quantified this observation in terms of the cell orientation with respect to the groove direction on the substrate.

Despite these growing observations of substrate topography governing the cytoskeletal arrangement within cells, no quantitative model to explain these

observations, including the so-called phenomenon of contact guidance, has been proposed to-date. Numerous numerical models have been proposed for the remodeling of the cytoskeleton in response to mechanical cues [17-20] and these have successfully predicted the response of cells on a bed of micro-posts [21], subjected to cyclic stretching [22] and other mechanical loadings such as indentations [23]. Some models have also coupled the stress fiber network with mechano-sensitive focal adhesion formation [24] and predicted the focal adhesion distributions on substrates with ligand patterns [25]. However, these models all impose an arbitrary spatially uniform activation signal for the cytoskeletal processes. This simplification makes these models unsuitable to predict the response of cells on nano-patterned substrates. Recall that cells sense the topography of their substrates via the feedback between intracellular signaling, cytoskeletal stress fiber formation and focal adhesion growth – this combination of mechanisms is critical when models are devised for understanding the development of the cytoskeleton on nano-patterned substrates. Here we use a co-operative feedback model proposed by Pathak et al. [26] in order to investigate the development of the stress fibers and focal adhesions for osteoblasts lying on grooved substrates as investigated by Lamers et al. [16].

2. Brief description of the bio-chemo-mechanical model

Pathak et al. [26] presented a framework for analyzing the co-operative feedback loop between signaling, focal adhesion formation, and cytoskeletal contractility. In the context of a cell placed on a substrate coated with ligands, this loop involves the following four steps:

Step 1. The placement of the cell on a substrate coated stimulates the formation of focal adhesions on the contact surfaces.

Step 2. The aggregation of proteins within the focal adhesion complexes triggers the cascade release of a range of signaling proteins and ions such as Rho, Src, and Ca^{2+}.

Step 3. These signaling molecules stimulate cytoskeletal contractility via the formation of actin/myosin stress fibers.

Step 4. The contractile forces generated by stress fibers apply tractions on focal adhesions, which induce further aggregation of integrins in focal adhesions, resulting in additional signaling cascades and consequent cytoskeletal rearrangements.

Here we briefly describe the relevant governing equations and the associated cellular processes in the context of a cell lying on a grooved substrate as in the experiments of Lamers et al. [16]. The substrate lies in the $x_1 - x_2$ plane (Fig. 1) and has grooves along the x_2-direction with a pitch L_0 in the x_1 direction. The ratio between the width w of the ridge and the pitch is denoted by $r \equiv w/L_0$. We envisage a two-dimensional (2D) cell, of thickness b (in x_3 direction) lying on this grooved substrate with adhesive contacts occurring *only along the ridges* (Fig. 1), i.e. the cell does not sink into the relatively deep grooves, in line with the experiments of Lamers et al. [16]. Thus, for purposes of modeling it suffices to think of a patterned substrate comprising of alternating strips to which the cell can adhere and strips where adhesion is prevented. The dimensions of the cell in the $x_1 - x_2$ plane are assumed to be $\gg L_0$ and here we aim only to model the response of a central portion of the cell far away from the periphery of the 2D cell. Thus, it suffices to model a one-dimensional (1D) unit cell of length L_0 as shown in Fig. 1 as (i) the response of the central portion of the cell is periodic with period L_0 and (ii) the state of the central portion of the cell is invariant in the x_2 direction with the strain rate $\dot{\varepsilon}_{22} = 0$ in the x_2-direction. The

precise boundary conditions will be made explicit subsequently and we now proceed to describe the relevant governing equations in this 1D context.

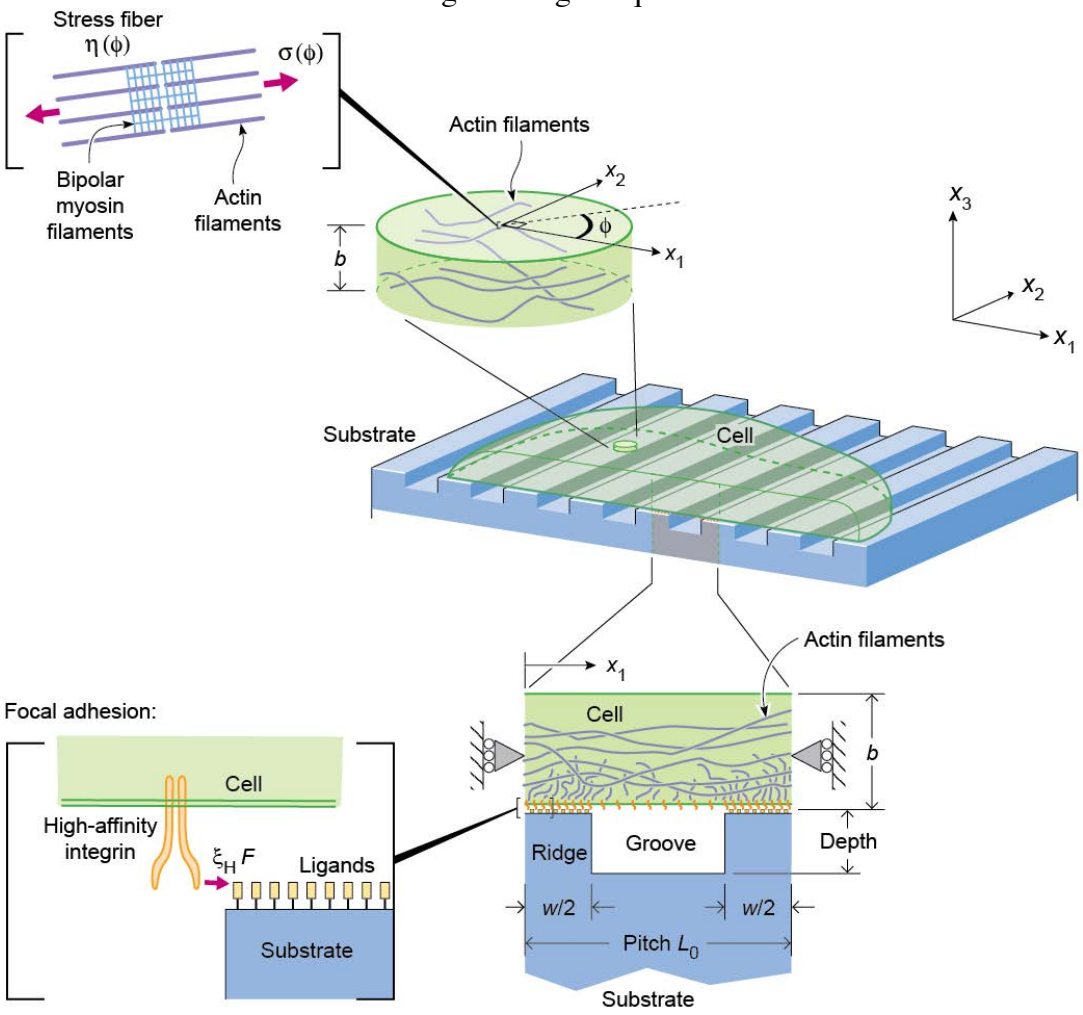

Figure 1: *Sketch of the two-dimensional cell on a grooved substrate. The network of stress fibers and the integrin–ligand complexes on the ridges are shown as insets along with the quasi one-dimensional periodic unit cell of the central portion of the cell analyzed in this study. The global co-ordinate system is indicated on the figures with the grooves aligned with the* x_2*-direction.*

The interaction of the cell with a substrate incorporates three components that link in a highly nonlinear manner: (i) the activation signal generation; (ii) stress fiber dynamics and (iii) focal adhesion dynamics. We shall briefly describe each of these components and readers are referred to the appropriate references quoted in each case for further details of the models.

Signal generation: Here we present the 1D version of the signaling model of Pathak et al. [26]. We emphasize here that details regarding the precise proteins involved in signaling are not crucial to the mathematical model described below. Rather, the emphasis is on the structure of the reaction-diffusion scheme that provides a positive feedback between focal adhesions and stress fiber formation. Thus, here we reinterpret the Ca^{2+} pathways discussed by Pathak et al. [26] in terms of signalling from focal adhesions through Rho GTPase and ROCK (Rho-associated protein kinase) with phosphorylation of NMM2 (non-muscle myosin II).

The main elements of signal activation and transduction phenomena modeled in the cell are: (a) activation of Rho due to the clustering of high affinity integrins, (b) simultaneous diffusion and de-phosphorylation of Rho molecules through the cell, (c) activation of ROCK by the Rho and finally (d) the activation of the intracellular contractile machinery, via ROCK. Processes (a) and (b) are captured via the reaction diffusion equation (overdot denoting differentiation with respect to time t)

$$\dot{S} = m_s kT \frac{\partial^2 S}{\partial x_1^2} - k_d S + \frac{\alpha}{b} \max\left(0, \dot{\xi}_H\right) - S\, \dot{\varepsilon}_{11}, \tag{2.1}$$

where the first term describes the diffusion of Rho through the cytosol, with S denoting the concentration of Rho in molecules per unit volume, m_s the mobility of Rho molecules in the cytosol, k is Boltzmann's constant, and T the absolute temperature. We assume that the de-phosphorylation of Rho is described by a first order reaction with a forward rate constant k_d and a negligible reverse reaction rate. This forward de-phosphorylation reaction is modeled by the second term in Eq. (2.1). The rate of activation of Rho at locations on the cell membrane where high affinity integrins cluster is described by the third term in Eq. (2.1). The rate of change of the concentration of high affinity integrins per unit cell membrane area is denoted by $\dot{\xi}_H$. An increment in ξ_H results in the activation of Rho with a non-dimensional proportionality constant α. Thus, α is interpreted as the number of Rho molecules activated when one low affinity integrin molecule is converted to its high affinity configuration[1]. It is worth reminding the readers here that adhesions only occur on the ridges and hence the activation of Rho as described by the third term in Eq. (2.1) is non-zero only along the ridges of the substrate. The final term describes the change in the concentration of Rho due to the change in the volume of the cytosol under strain. In this 2D setting, the volumetric strain rate reduces to $\dot{\varepsilon}_{11}$, the strain rate in the x_1 direction, as $\dot{\varepsilon}_{22} = 0$ and the 3rd direction is neglected in this analysis.

The Rho diffusing through the cytosol activates ROCK which is also being simultaneously deactivated as it intramolecularly refolds (i.e. process (c) mentioned above). We express these kinetics in terms of the normalized activated ROCK concentration $0 \leq C \leq 1$, where C is the ratio of the activated ROCK concentration to the maximum allowable concentration. Assuming first order kinetics, the rate of change of C at any location in the cytosol is given as

$$\dot{C} = \lambda_f \frac{S}{S_0}(1 - C) - \lambda_b C, \tag{2.2}$$

where λ_f is the rate constant governing the unfolding of the ROCK by Rho and S_0 is a reference concentration of Rho. The rate constant λ_b governs the rate at which ROCK is refolded. The kinetic relation provides the value of the signal C at any location in the cytosol to initiate cytoskeletal stress fiber rearrangement; i.e., this is the input to a stress fiber contractility model.

[1] Note that the transformation of integrins from the high affinity to the low affinity state (resulting in a negative $\dot{\xi}_H$) does not contribute toward Rho activation.

Stress-fiber contractility model: The bio-chemo-mechanical model of Deshpande et al. [17] captures the formation and dissociation of stress fibers, as well as the associated generation of tension and contractility. In this model, actin polymerization (leading to stress-fiber formation in the cell) is governed by three coupled phenomena: (i) an activation signal, (ii) tension-dependent stress-fiber kinetics, and (iii) a force generation mechanism governed by cross-bridge cycling between actin and myosin filaments.

The formation of stress fibers is parameterized by an activation level, designated as η $(0 \leq \eta \leq 1)$ defined as the ratio of the concentration of the polymerized actin and phosphorylated myosin within a stress fiber bundle to the maximum concentrations permitted by biochemistry. The evolution of $\eta(\phi)$ in a direction ϕ with respect to the x_1 axis (Fig. 1) is characterized by a first order kinetic equation,

$$\dot{\eta}(x_1, \phi, t) = k_f C[1 - \eta(x_1, \phi, t)] - k_b \left[1 - \frac{\sigma(x_1, \phi, t)}{\sigma_0(x_1, \phi, t)}\right] \eta(x_1, \phi, t), \tag{2.3}$$

where k_f and k_b are the forward and backward rate constants, respectively. In this formula, σ is the tension in the stress fiber bundle oriented at angle ϕ while $\sigma_0 \equiv \eta\sigma_{max}$ is the corresponding isometric tension. The stress σ is related to the fiber contraction/extension strain rate $\dot{\varepsilon}(\phi)$ by the cross-bridge cycling between the actin and myosin filaments. A simplified (but adequate) version of the Hill [27] equation is employed to model these dynamics and is specified as

$$\frac{\sigma}{\sigma_0} = \begin{cases} 0 & \frac{\dot{\varepsilon}}{\dot{\varepsilon}_0} < -\frac{\eta}{k_v} \\ 1 + \frac{k_v \dot{\varepsilon}}{\eta \dot{\varepsilon}_0} & -\frac{\eta}{k_v} \leq \frac{\dot{\varepsilon}}{\dot{\varepsilon}_0} \leq 0 \\ 1 & \frac{\dot{\varepsilon}}{\dot{\varepsilon}_0} > 0, \end{cases} \tag{2.4}$$

where the rate sensitivity coefficient, k_v is the fractional reduction in fiber stress upon increasing the shortening rate by $\dot{\varepsilon}_0$. Moreover, the fiber strain rate $\varepsilon(\dot{\phi})$ is related to the material strain rate via $\dot{\varepsilon} = \dot{\varepsilon}_{11}\cos^2\phi$ as $\dot{\varepsilon}_{22} = \dot{\varepsilon}_{12} = 0$ and the average stress generated by the fibers then follows from a homogenization analysis as

$$\begin{pmatrix} \sigma_{11} & \sigma_{12} \\ \sigma_{12} & \sigma_{22} \end{pmatrix} = \frac{1}{\pi} \int_{-\pi/2}^{\frac{\pi}{2}} \begin{pmatrix} \sigma \cos^2\phi & \frac{\sigma}{2}\sin 2\phi \\ \frac{\sigma}{2}\sin 2\phi & \sigma \sin^2\phi \end{pmatrix} d\phi. \tag{2.5}$$

The constitutive description for the stress state within the cell is completed by including contributions from passive elasticity, attributed to intermediate filaments and microtubules of the cytoskeleton attached to the nuclear and plasma membranes. These act in parallel with the active elements, whereupon additive decomposition gives the total stress as

$$\Sigma_{ij} = \sigma_{ij} + \sigma_{ij}^{P}, \tag{2.6}$$

with the passive stress σ_{ij}^{P} assumed to be given by a 2D neo-Hookean elasticity model parameterized by the Young's modulus E and Poisson's ratio ν. In terms of the two in-plane principal stretches λ_i the two in-plane principal passive stresses σ_i^p (corresponding to the stress σ_{ij}^{P}) are given as

$$\sigma_i^p = \frac{E}{4(1+\nu)} J^{-2}(2\lambda_i^2 - I_1) + \frac{E}{2(1-\nu)}(J-1), \tag{2.7}$$

where $I_1 = \lambda_1^2 + \lambda_2^2$ and $J = \lambda_1\lambda_2$. Note that in the unit cell described above, x_1 and x_2 are principal directions and $\lambda_2 = 1$ which greatly simplifies the calculation of σ_{ij}^{P} from Eq. (2.7). We note here that for simplicity we only include elastic passive stresses and neglect any viscoelastic effects. This simplification suffices in this study where the focus is on the steady-state response of the cells: at steady-state viscoelastic effects have decayed away and only the elastic passive stresses persist.

Focal adhesion model: Deshpande et al. [24] presented a thermodynamically motivated model for the mechano-sensitive formation (and dissociation) of focal adhesions. The model relies on the existence of two conformational states for the integrins: low and high affinity states. Only the high-affinity integrins interact with the ligand molecules on the ECM to form complexes. The low-affinity integrins remain unbonded. Since the formation (or dissociation) of the FAs depends on the relative stabilities of the high- and low-affinity integrins, we examine the thermodynamic equilibrium of the two states, which we model as an ideal mixture. The chemical potential of the low-affinity integrins at concentration ξ_L is dependent on their internal energy and configurational entropy in accordance with

$$\chi_L = \mu_L + kT \ln(\xi_L/\xi_R), \tag{2.8}$$

where μ_L is the reference potential of the low-affinity integrins and ξ_R their reference concentration. For geometrical reasons, the straight architecture of the high-affinity integrins permits the interaction of its receptor with the ligand molecules on the ECM, and allows the force transmission between the cell and the substrate. Thus, the high-affinity integrins have an additional contribution to their chemical potential, due to the elastic energy of the integrin–ligand complexes. The ensuing potential is

$$\chi_H = \mu_H + kT \ln(\xi_H/\xi_R) + \Phi(\Delta) - F\Delta, \tag{2.9}$$

where $\mu_H > \mu_L$ is the reference potential of the high-affinity integrins and $\Phi(\Delta)$ the

stretch energy stored in the integrin ligand complex stretched by Δ via a force $F \equiv \partial\Phi/\partial\Delta$. Spatial gradients in the foregoing chemical potentials motivate the fluxes of the integrins. Two kinetic processes are involved: (i) those governing the rate of conversion of the low-affinity integrins to their high-affinity state (and vice versa) and (ii) diffusive fluxes of the low-affinity integrins along the plasma membrane. The kinetic process (i) is typically fast compared with all other time scales involved and hence we assume local thermodynamic equilibrium between the low and high affinity states such that $\chi_H = \chi_L$, while the trafficking of the low affinity is governed by the diffusion equation

$$\dot{\xi} = m\frac{\partial}{\partial x_1}\left(\xi_L \frac{\partial \chi_L}{\partial x_1}\right) - \xi\,\dot{\varepsilon}_{11}, \tag{2.10}$$

where $\xi = \xi_L + \xi_H$ and m is the mobility of the low affinity integrins along the cell membrane. It now remains to specify the form of the stretch energy $\Phi(\Delta)$ and the relation of Δ to the displacement u_1 of the 1D cell. Rather than employing a complex interaction, such as the Lennard-Jones potential [28] we use a simple functional form which is a piecewise quadratic potential expressed as

$$\Phi = \begin{cases} \frac{1}{2}\kappa_s \Delta^2 & \Delta < \Delta_n \\ \kappa_s\left(2\Delta_n\Delta - \Delta_n^2 - \frac{1}{2}\Delta^2\right) & \Delta_n \le \Delta \le 2\Delta_n \\ \kappa_s\Delta_n^2 & \Delta > 2\Delta_n, \end{cases} \tag{2.11}$$

where $\gamma \equiv \Phi(\Delta \to \infty) = \kappa_s\Delta_n^2$ is the surface energy of the high-affinity integrins and κ_s the stiffness of the integrin-ligand complex. The maximum force in the integrin-ligand complex, $\kappa_s\Delta_n$ occurs at a stretch $\Delta = \Delta_n$. Finally, the evolution of the stretch Δ is related to the displacement u_1 of the material point on the cell membrane in contact with the ligand patch on the rigid substrate via

$$\dot{\Delta} = \begin{cases} \dot{u}_1 & \Delta < \Delta_n \ \text{ or } \ F\dot{\Delta} < 0 \\ 0 & \text{otherwise.} \end{cases} \tag{2.12}$$

where $\dot{\varepsilon}_{11} = \partial\dot{u}_1/\partial x_1$.

Mechanical equilibrium: Mechanical equilibrium of the 1D cell stipulates that

$$b\frac{\partial \Sigma_{11}}{\partial x_1} = \xi_H F, \tag{2.13}$$

for the portion of the cell along where adhesions occurs (i.e. along the ridges of the grooved substrate) and F is the force exerted by the cell on the integrin-ligand complex. On the portion of the cell that cannot form adhesions (i.e. the portion of the cell over the grooves), $\partial\Sigma_{11}/\partial x_1 = 0$. Thus, the total stress Σ_{11} is spatially uniform

over the portion of the cell lying over the grooves.

Initial and boundary conditions: We analyze a 1D unit cell of length L_0 as sketched in Fig. 1 with $x_1 = 0$ corresponding to the left edge. The boundary conditions for the mechanical equilibrium Eq. (2.13) follow from periodicity as $u_1 = 0$ at $x_1 = 0$ and $x_1 = L_0$. In addition, we assume the state of the central portion of the cell to be invariant in the x_2-direction and thus impose $\varepsilon_{22} = 0$ throughout the cell. Periodicity also dictates that there is no net flow of the activated Rho or the low affinity integrins out of the unit cell and thus the boundary conditions to Eqs. (2.1) and (2.10) are $\partial S/\partial x_1 = 0$ and $\partial \xi_L/\partial x_1 = 0$, respectively at $x_1 = 0$ and $x_1 = L_0$.

For simplicity we assume that the cell is stress, stress-fiber and activation signal free at time $t = 0$ which implies that initially $u_1 = \dot{u}_1 = \dot{\varepsilon}_{11} = \eta(\phi) = C = \Sigma_{11} = 0$ throughout the cell. It now remains to specify an initial spatial distribution of the low and high affinity integrins. At time $t = 0^-$, the cell is not in contact with the grooved substrate and low and high affinity integrins are uniformly distributed over the cell membrane. In this case, the bond stretch $\Delta \to \infty$ such that $F = 0$ and $\Phi = \gamma$. Then, over the entire surface of the cell, equilibrium between the low and high affinity integrins specifies

$$\xi_H = \frac{\xi_0}{\exp\left[\frac{\mu_H - \mu_L + \gamma}{kT}\right] + 1}, \tag{2.14}$$

where $\xi_0 = \xi_L + \xi_H$ is the total integrin concentration at any location on the cell membrane. At time $t = 0^+$, the cell is placed on the grooved substrate which changes the bond stretch to $\Delta = 0$ (and $\Phi = 0$) for the high affinity integrins in contact with the substrate. Thus, at time $t = 0^+$, the spatial distribution of the integrins is non-uniform and given by Eq. (2.14) over the domain $w/2 < x_1 < L_0 - w/2$ (i.e. the portion of the cell over the groove where no adhesions form) and by

$$\xi_H = \frac{\xi_0}{\exp\left[\frac{\mu_H - \mu_L}{kT}\right] + 1}, \tag{2.15}$$

with $\xi_L = \xi_0 - \xi_H$ at locations along the ridges where adhesions form (i.e. over the domains $0 \le x_1 \le w/2$ and $L_0 - w/2 \le x_1 \le L_0$). The increase $\Delta\xi_H$ in the concentration of the high affinity integrins along the ridges, given by the difference in the values of ξ_H between Eqs. (2.15) and (2.14), will result in Rho activation in the portion of the cell in contact with the substrate. Thus, the initial conditions for S follow as $S = 0$ over $w/2 < x_1 < L_0 - w/2$ and $S = (\alpha/b)\,\Delta\xi_H$ over the domains $0 \le x_1 \le w/2$ and $L_0 - w/2 \le x_1 \le L_0$. These initial spatial gradients in the integrin concentrations and the initial development of S due to the action of placing the cell on the substrate will drive the subsequent production of stress fibers, additional focal adhesion formation and signaling via the co-operative model detailed above without the need for any artificial external stimuli. The model thus includes both the local and global interactions referred to in Oakes and Gardel [29]: the local forces cause adhesion growth and signaling but these forces are in turn determined by

global mechanical equilibrium considerations.

The numerical technique used to solve the above set of coupled partial differential equations is briefly described in the Supplementary material.

2.1 Review of the model assumptions

The model makes a number of key assumptions in order to make the problem mathematically and numerically tractable. Here we review some of the key assumptions in view of providing some justifications:

(i) We model the cell using a quasi 1D assumption. This considerably simplifies the solution of the complex coupled equations but also allows for easier interpretation of the results. The 1D assumption which only models the interior of the cell neglects the process of cell spreading that occurs during the early phase of the response of cells on patterned substrates [30]. Moreover, this approach also does not include the differences in adhesions [30] and stress fibers [31] structures between the cell interior and periphery. Thus, the model is restricted to steady-state response of the cell interior.

(ii) We restrict attention to cases where the cell membrane does not dip into and form adhesions within the grooves. Lamers et al. [16] show this to be true for grooves with depths ≥ 33 nm. With the effect of the migration of the cell membrane into the grooves neglected, the modeling of the response of cells on grooved substrates reduces to that of cells on patterned substrates where cells only form adhesions on patches that represent the ridges.

2.2 Material and substrate parameters

All simulations are reported for cells of thickness $b = 1\ \mu\text{m}$ at a temperature $T = 310\ \text{K}$ with the period L_0 of the grooves varied as a parameter over the range $0.05\ \mu\text{m} \leq L_0 \leq 2.0\ \mu\text{m}$. Unless otherwise specified we keep the ratio $r \equiv w/L_0 = 0.5$ as in the experiments of Lamers et al. [16] and assume the substrates to be rigid. Parameters for the signaling model are inferred from [32] to be: the reference Rho concentration $S_0 = 1000$ molecules μm^{-3} (i.e. $\sim 2\ \mu\text{M}$) with the proportionality constant $\alpha = 1.75$. The mobility of Rho is extremely high with $m_s = 10^4 \text{s mg}^{-1}$. Moreover, the unfolding of ROCK by Rho is very rapid but the refolding of ROCK is relatively slow and thus we assume $\lambda_f \gg \lambda_b$, with $\lambda_f = 2.5\times10^5\ \text{s}^{-1}$ and $\lambda_b = 0.015\ \text{s}^{-1}$. The reference value of the rate constant governing the de-phosphorylation of Rho is taken as $k_d = 750\ \text{s}^{-1}$ but we report simulations where this parameter is varied to investigate the sensitivity of the results to k_d. The parameters for the focal adhesion model are obtained from [33-36]. The resting integrin concentration is $\xi_0 = 1000$ integrins μm^{-2} and the difference in the reference potentials between the high and low affinity integrins is taken to be $\mu_H - \mu_L = 5kT$. The mobility of the low affinity integrins is significantly less than Rho with $m = 10\ \text{s mg}^{-1}$ while the stiffness of the high affinity/ligand bonds is $\kappa_s = 15\ \text{pN}\ \mu\text{m}^{-1}$ with a peak force $\kappa_s \Delta_n = 1.95\ \text{pN}$. The parameters for the cellular contractility model are taken based on the calibrations performed by McGarry et al. [21] for osteoblasts with a passive elastic modulus $E = 4\ \text{kPa}$ and $\nu = 0.45$. The maximum stress fibre stress is $\sigma_{max} = 2.5\ \text{kPa}$ while the Hill model parameters are $k_v = 3$ and $\dot{\varepsilon}_0 = 2.8\times10^{-4}\ \text{s}^{-1}$. The rate constants for the stress fiber kinetics are $k_f = 0.03\ \text{s}^{-1}$ and $k_b = 0.1k_f$.

3. Simulations of cell response on grooved substrates

The action of placing the cell on the grooved substrate initiates the signaling process that prompts the cascade of contractility, focal adhesion formation and further signaling as described above. The model parameters listed in Section 2.1 result in processes occurring over three time-scales: (i) the diffusion of the Rho that occurs on the order of a few milliseconds; (ii) the unfolding of ROCK that occurs on the same time-scale as the Rho diffusion, but its refolding and consequent de-activation occurs on the order of a few minutes and (iii) the stress fiber kinetics that occur on the order of hours. While we do not model the cell periphery where the short-time scale processes dominate we emphasize here that these fast Rho diffusion and ROCK activation processes are the key triggers for the slower stress fiber kinetic processes in the interior of the cell modeled here. We now proceed to discuss these processes for the two extreme values of $L_0 = 0.05$ μm and 1 μm so as to first explain two extreme types of responses.

First consider the early time response on the order of a few milliseconds. In this time-scale there is no significant evolution of the focal adhesions or stress fibers while the activated Rho and unfolded ROCK concentrations have responded to the action of the placement of the cell on the grooved substrate. The spatial distributions of S/S_0 and C are included in Figs. 2a and 2b for the $L_0 = 0.05$ μm and 1 μm cases, respectively. In each case predictions are shown for three selected values of time t, where $t = 0$ corresponds to the instant the cell was placed on the substrate. First consider the $L_0 = 0.05$ μm case. At time $t = 0^+$ the initial condition described above implies that $S = \alpha\Delta\xi_H/b$ over the domains $0 \leq x_1/L_0 \leq 0.25$ and $0.75 \leq x_1/L_0 \leq 1$ and $S = 0$ over the central section where the cell covers the groove. Subsequently, the Rho begins to rapidly diffuse towards the central section while it is simultaneously being de-phosphorylated at the rate $k_d S$. This is clearly seen in Fig. 2a where the concentration S is reducing across the portion of the cell over the ridges but increasing over the portion of the cell above the grooves. However, for $t > 2.0$ ms, the de-phosphorylation rate even in this central section becomes higher than the influx rate of the Rho and the concentration S decreases throughout the cell and reduces to zero everywhere for $t \geq 3.5$ ms. We note that at these early times there is nearly no response from the stress fibers, hence no new focal adhesions form and thus there is no further Rho activation. Now consider the corresponding evolution of the unfolded ROCK concentration. At time $t = 0$, $C = 0\ \forall x_1$ and then begins to rise in response to the local Rho concentration. The kinetics of ROCK is slower and hence the ROCK concentration continues to increase even as the Rho concentration decreases and begins to become more spatially uniform. Over the time-scale of Fig. 2a, the process of refolding of ROCK has no significant effect and hence C has not begun to decrease. The evolution of S and C for the $L_0 = 1$ μm case is similar with once major difference. The large length implies that the Rho is de-phosphorylated prior to it reaching the central portion of the cell over the groove. Thus, both S and C are approximately zero over the section $0.25 < x_1/L_0 < 0.75$ (expect for a small boundary layer near the edges of the ridges).

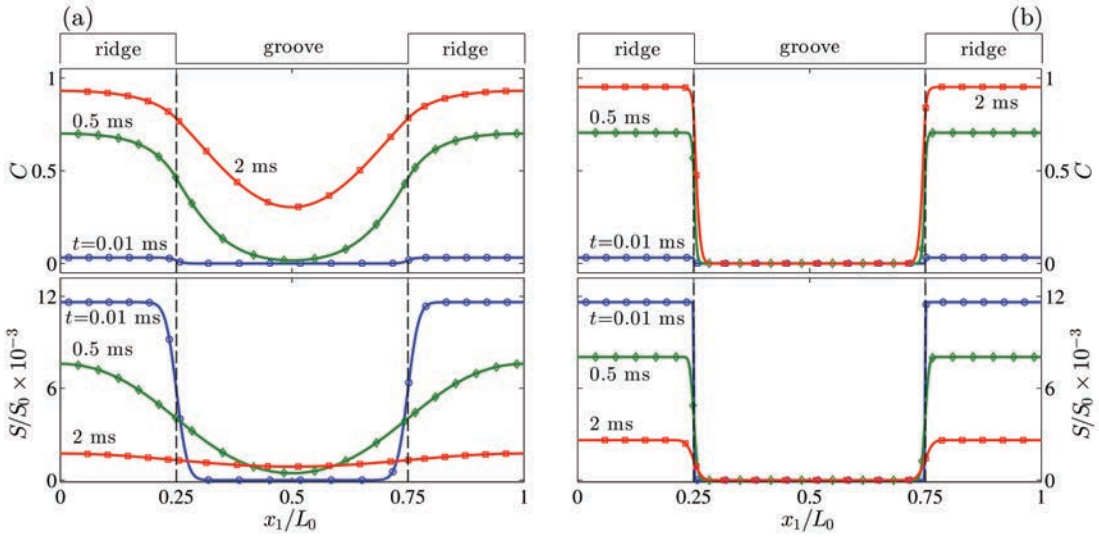

Figure 2: *The spatial distributions of the signal levels* S/S_0 *and* C *at three selected times* $t \leq 2$ *ms for the cells on substrates with pitches (a)* $L_0 = 0.05\ \mu m$ *and (b)* $L_0 = 1\ \mu m$. *Time* $t = 0$ *corresponds to the instant the cell was placed on the substrate.*

Now consider the response over the time frame of minutes when $S \approx 0$ due to it having been largely de-phosphorylated. In Fig. 3 we plot predictions of the spatial distributions of C, the focal adhesions as parameterized by ξ_H/ξ_0, the strain rate $\dot{\varepsilon}_{11}/\dot{\varepsilon}_0$ and the stress fiber concentrations η_0 and η_{90} in the $\phi = 0^o$ and $\phi = 90^o$, respectively for three selected values of the time t. First consider the $L_0 = 0.05$ µm case in Fig. 3a. The ROCK concentration C is spatially relatively homogenous and decreases throughout the cell over the time scales shown here. On the other hand, the focal adhesions, as parameterized by the normalized concentration ξ_H/ξ_0, are spatially uniform over the ridges (and approximately zero over the grooves where no adhesions form) and do not change on the time scale of the plots in Fig. 3a. This is consistent with the observation that $\dot{\varepsilon}_{11} \approx 0$ over the ridges which implies that there is no additional stretching of the integrin-ligand bonds over these time-scales and therefore the focal adhesions are reasonably static. However, tensile strain rates are present in the central portion of the cell over the grooves for $t \leq 3$ min, balanced by small contractile strain rates over the remainder of the cell as the total length of the portion analyzed does not change. The stress fiber distributions are reasonably isotropic with $\eta_0 \approx \eta_{90}$ throughout the cell though the stress fiber concentrations are slightly lower in the central portion due to the lower levels of signal C in this part of the cell.

Now consider the $L_0 = 1$ µm case in Fig. 3b. Recall that the Rho does not diffuse into the central portion of this cell over the groove. Thus, the ROCK concentration C, as well as the stress fiber concentrations, η_0 and η_{90}, vanish over this central section. The absence of stress fibers results in tensile strain rates over the central section and corresponding contractile rates $\dot{\varepsilon}_{11}$ over the ridges where stress fibers form and contract. These strain rates result in stretching of the integrin-ligand bonds especially near the edges of the ridges at the larger values of t (e.g. $t = 12$ min in Fig. 3b), producing both an increase in the focal adhesion concentration at those locations and a corresponding rise in the ROCK concentration C. Consider now the stress fibers

kinetics. Stress fibers in this case only form on the ridges where there exists a non-zero signal. Early in the deformation history (i.e. $t = 0.5$ min) the stress fiber distributions on the ridges are nearly isotropic with $\eta_0 \approx \eta_{90}$. However, as time proceeds the fibers in the $\phi = 0^o$ direction dissociate due to the contractile strain rates $\dot{\varepsilon}_{11}$ (and relatively low values of C) but the fibers in the $\phi = 90^o$ direction continue to form due to a low persistent signal C and aided by the fact that the dissociation rate in this direction is zero as $\dot{\varepsilon}_{22} = 0$.

A more complete history of the evolution of $C, \xi_H/\xi_0, \dot{\varepsilon}_{11}/\dot{\varepsilon}_0$ as well as η_0 and η_{90} are shown in Figs. 4a and 4b, respectively for the $L_0 = 0.05$ μm and 1 μm cases. Contours of the distributions of these quantities are shown in Fig. 4 where the horizontal axes indicates the time (now in units of hours), while on the vertical axes we plot the normalized position x_1/L_0. For the $L_0 = 0.05$ μm case it is clear that the signal C has decayed early in the time history ($t \leq 0.05$ h) and the focal adhesions too have attained their final distribution very early. However, the stress fiber concentration η_{90} attains its steady value over a time of about 0.12 h due to the slower kinetics of the stress fiber formation. The relaxation rates implicit within the Hill-relation are even slower, which implies that the strain rate $\dot{\varepsilon}_{11}$ drops to zero over a time scale of about 0.5 h and thus this is also the time-scale over which η_0 attains its steady-state value. Qualitatively this time history is similar to the $L_0 = 1$ μm case (Fig. 4b), with two major caveats: (i) the presence of the unfolded ROCK is clearly restricted to the ridges, and the additional stretching of the integrin-ligand bonds due to the longer groove spacing results in additional signal generation[2], and (ii) this additional signaling takes place on the time-scale of stress fiber contraction, which delays the attainment of steady-state in the $L_0 = 1$ μm case to nearly 1 hour. In this context recall that the analysis reported here only models the central portion and not the periphery of the cell. Thus, consistent with observations the model predicts that nearly no adhesions form in the central portion of cell for substrates with $L_0 = 0.05$ μm other than those formed at time $t = 0^+$ by the action of placing the cell on the substrate (the cell periphery where adhesions are observed in such cases is not modeled here). On the other hand, adhesions form over a time scale of approximately 0.5 hours in the central portion of cells on the $L_0 = 1$ μm substrates. This slow adhesion growth is consistent with observations [30] for cells on patterned substrates.

[2] We make the contribution of the additional signal generation explicit in the supplementary material.

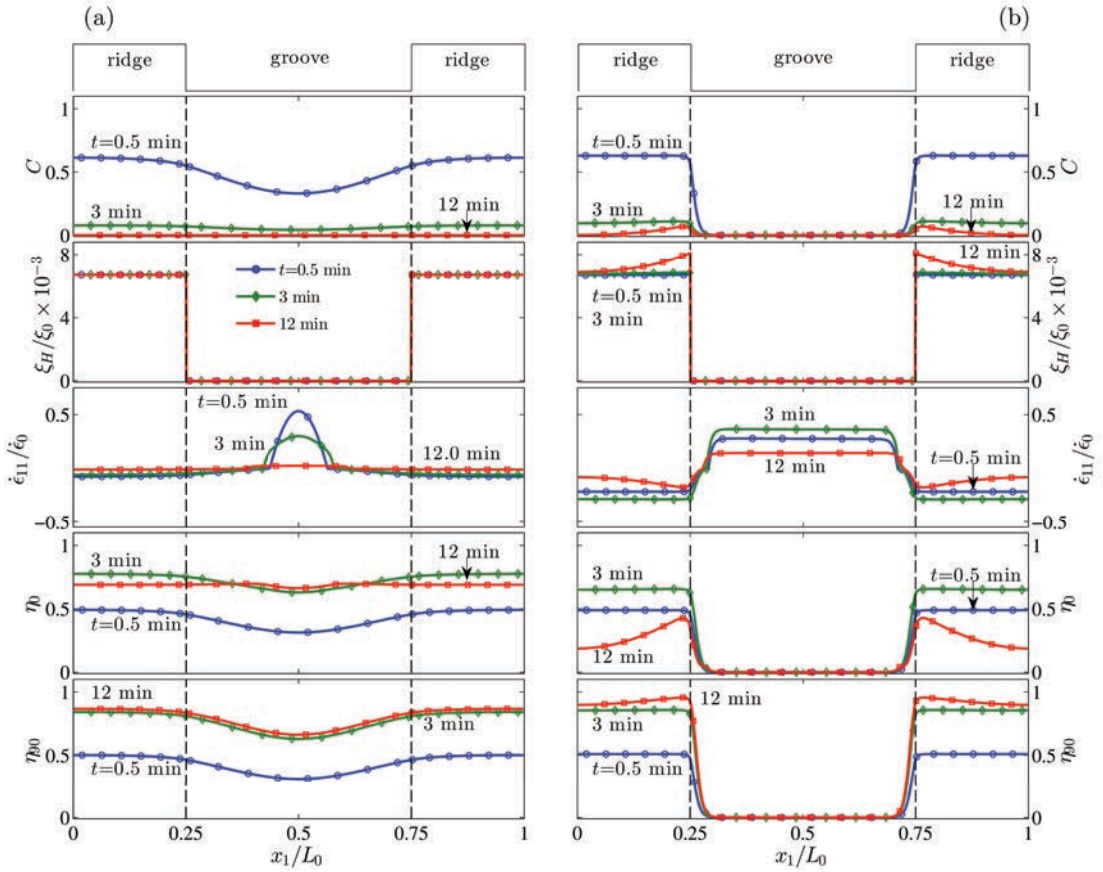

Figure 3: *The spatial distributions of* C, ξ_H/ξ_0, $\dot{\varepsilon}_{11}/\dot{\varepsilon}_0$ *as well as the stress fiber concentrations* η_0 *and* η_{90} *for three selected values of the time* $t \leq 12$ *min for cells on substrates with pitches (a)* $L_0 = 0.05\ \mu m$ *and (b)* $L_0 = 1\ \mu m$. *Time* $t = 0$ *corresponds to the instant the cell was placed on the substrate.*

The steady-state spatial distributions of stress fiber concentrations, η_0 and η_{90}, are included in Figs. 5a and 5b for the $L_0 = 0.05$ μm and 1 μm cases, respectively. Also included in Fig. 5 are insets showing circular histograms (similar to those introduced in [22, 37]) of η at three locations along the cell: $x_1/L_0 = 0.125$ (mid-point of the ridge); $x_1/L_0 = 0.25$ (edge of the ridge) and $x_1/L_0 = 0.5$ (mid-point of the groove). These histograms visually quantify the degree of anisotropy in the distribution of the stress fibers. Clearly for the $L_0 = 0.05$ μm case the steady-state distribution of the stress fibers is both nearly isotropic and spatially uniform. This implies that stress fibers form not only along the ridges but also bridge across the grooves from ridge-to-ridge as seen in Fig. 4c of Lamers et al. [16]. By contrast, the steady-state distribution of the stress fibers in the $L_0 = 1$ μm case is both anisotropic and spatially inhomogeneous with fibers only forming on the ridges. On these ridges the angular distribution of fibers shows a higher concentration in the $\phi = 90^o$ direction and almost no stress fibers forming in the $\phi = 0^o$ direction. This lower concentration of η_0 is due to the fact that the Rho is de-phosphorylated before it can reach the central portion of the cell over the groove, which prevents the formation of a stable stress fiber bundle across grooves as in the $L_0 = 0.05$ μm case. This implies that stress fibers forming over the ridges at $\phi = 0^o$ contract as there are no stress fibers in the cell over the groove to balance their contractile forces. This contraction results in the dissociation of the stress fibers in the $\phi = 0^o$ direction, and consequently lower concentrations of η_0 remain above the ridges at steady state. It is worth emphasizing

here that unlike in the $L_0 = 0.05$ μm case, stress fibers do not bridge over the grooves in the $L_0 = 1$ μm case. Thus, long continuous stress fibers will primarily be observed only around the $\phi = 90^o$ direction over the ridges for cells on the $L_0 = 1$ μm substrates.

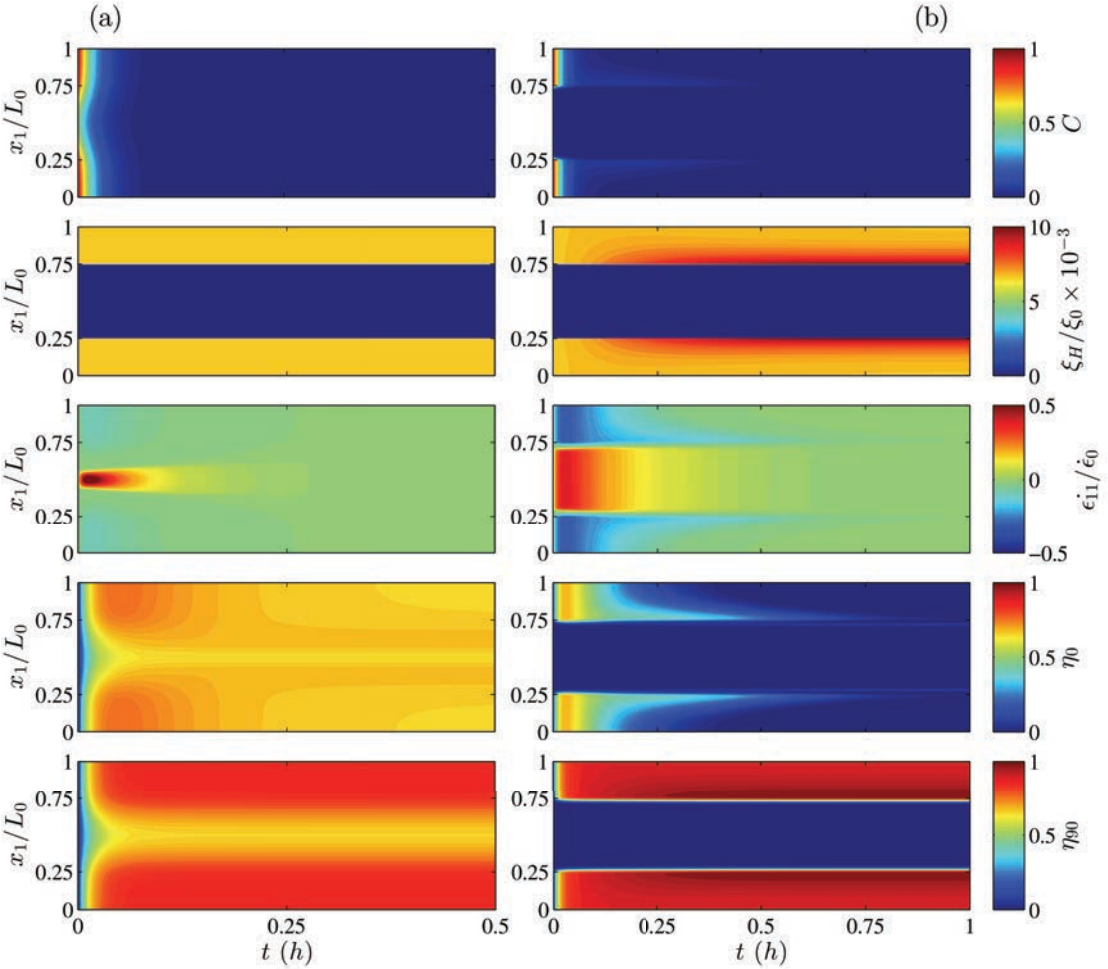

Figure 4: *Contour plots of the spatio-temporal distributions of* C, ξ_H/ξ_0, $\dot{\varepsilon}_{11}/\dot{\varepsilon}_0$ *as well as* η_0 *and* η_{90} *for cells on substrates with pitches (a)* $L_0 = 0.05\ \mu$m *and (b)* $L_0 = 1\ \mu$m *during transient. Time* $t = 0$ *corresponds to the instant the cell was placed on the substrate. Recall that the groove spans the range* $0.25 \leq x_1/L_0 \leq 0.75$.

Animations showing the evolution of the C, ξ_H/ξ_0, $\dot{\epsilon}_{11}/\dot{\epsilon}_0$, η_0 and η_{90}, as well as the circular the distribution of η at selected locations within the cells are included in the supplementary material files.

3.1 Predictions of cell alignment and comparisons with measurements

One of the key findings of the experiments of Lamers et al. [16] was the change in the cell orientation as a function of the groove width L_0. In order to quantify cell orientation Lamers et al. [16] fluorescently stained the actin filaments and then measured the orientation of the dominant actin filaments with respect to the ridge direction. We denote this orientation as Ω and replot the measured median values of Ω as a function of L_0 in Fig. 6a. In Fig. 6a a non-linear x-axis scale, $\sqrt{L_0}$, has been employed in order to improve the visualization of the data. A median value of $\Omega = 45^o$ indicates a random orientation while $\Omega = 0^o$ indicates that the cells are

primarily aligned with the ridge (or groove) directions. The measurements clearly show that while cell orientation is random for $L_0 \leq 0.1$ μm, there is a sharp transition at $L_0 \approx 0.1$ μm with the cells being primarily aligned with the ridge direction at higher values of L_0.

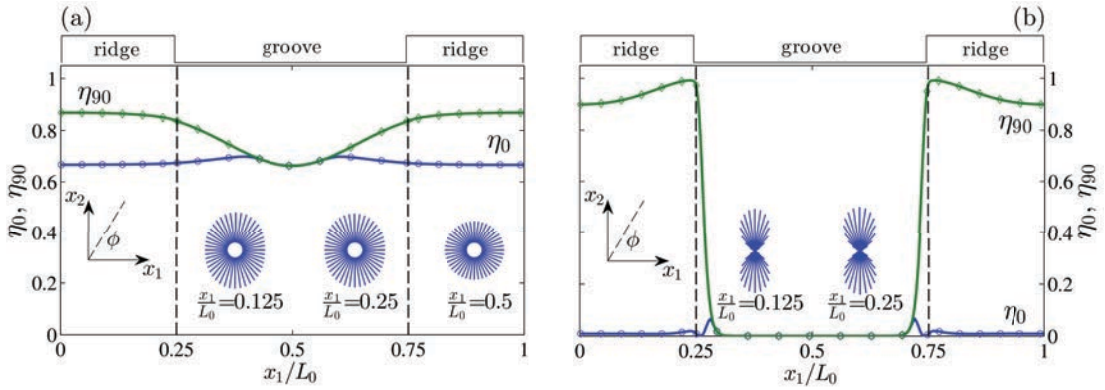

Figure 5: *The spatial distributions of the stress fiber concentrations* η_0 *and* η_{90} *at steady-state for cells on substrates with pitches (a)* $L_0 = 0.05$ μm *and (b)* $L_0 = 1$ μm. *Circular histograms of* η *at steady-state are included as insets at three selected locations within the cell. The histogram at* $x_1/L_0 = 0.5$ *is omitted in (b) as* $\eta \approx 0 \; \forall \; \phi$ *in this case.*

The model predictions discussed above clearly indicate that the cells form nearly isotropic stress fiber distributions at small values of L_0, but form anisotropic distributions with high stress fiber concentrations in the $\phi = 90^o$ direction (i.e. aligned with the ridge direction) for large values of L_0. This indicates that the model is predicting cell orientations that are at least qualitatively consistent with the observations of Lamers et al. [16]. In order to make more quantitative comparisons we attempt to interpret the predictions of the model in a manner analogous to the observations reported by Lamers et al. [16]. We first define an average stress fiber concentration in any particular direction as

$$\bar{\eta}_\phi \equiv \frac{1}{L_0}\int_0^{L_0} \eta(\phi) dx_1. \tag{3.1}$$

Predictions of $\bar{\eta}_\phi$ as function of $\pi/2 - \phi$ are plotted in Fig. 6b for selected values of L_0 (we choose the abscissa of $\pi/2 - \phi$ rather than ϕ so as to be consistent with the definition of cell orientation Ω employed by Lamers et al. [16]). It is clear that for small values of L_0, $\bar{\eta}_\phi$ is reasonably independent of ϕ but at larger values of L_0, $\bar{\eta}_\phi$ decreases sharply with increasing $\pi/2 - \phi$. Moreover, the $\bar{\eta}_\phi$ distributions are reasonably insensitive to the value of L_0 for $L_0 > 0.25$ μm. Thus, consistent with the experimental observations, the predictions in Fig. 6b suggest that the cell has stress fibers over the entire range of orientations, but some orientations are dominant with higher values of $\bar{\eta}_\phi$. It thus remains to quantity these dominant orientations in a manner as analogous as possible to the procedure employed by Lamers et al. [16].

In cell observations using epifluorescence or confocal microscopes, the fine meshwork of actin is expected to not be visible, i.e. if $\bar{\eta}_\phi$ is less than a critical value, fibers in that orientation are likely to be missed in most observations. We define this

critical value of $\bar{\eta}_\phi$ above which fibers are visible to be 50% of the maximum value, i.e. only fibers with $\bar{\eta}_\phi \geq 0.5$ will be visible. Now define a new observable stress fiber distribution as

$$\Gamma_\phi \equiv \begin{cases} \bar{\eta}_\phi & \bar{\eta}_\phi \geq 0.5 \\ 0 & \text{otherwise.} \end{cases} \tag{3.2}$$

Then, similar to Lamers et al. [16], the cell orientation Ω is defined as the mean value

$$\Omega = \frac{\pi}{2} - \frac{\int_0^{\pi/2} \phi \Gamma_\phi d\phi}{\int_0^{\pi/2} \Gamma_\phi d\phi}. \tag{3.3}$$

The predicted values of cell orientation using this definition of Ω are included in Fig. 6a for three selected values of the de-phosphorylation rate constant k_d, including the reference value of $k_d = 750\ \mathrm{s}^{-1}$. It is clear that the predictions are in reasonable agreement with the measurements for k_d values in the range $500\ \mathrm{s}^{-1} \leq k_d \leq 750\ \mathrm{s}^{-1}$. Recall that there are some uncertainties of the model parameters and the metrics used to compare the predictions and observations. Given these uncertainties the key conclusion of the model is that the lower limit of the groove spacing for an interaction between the grooves and the cells is $L_0 \approx 0.1$ μm but the interaction is definitely lost with cells orienting randomly on substrates for groove spacings $L_0 < 50$ nm.

The predictions in Fig. 6a extend to values of L_0 higher than those investigated by Lamers et al. [16]. These predictions seem to indicate that at $L_0 > 1$ μm, the cells will slowly begin to reorient themselves away from the ridge directions. We demonstrate in the supplementary material that this reorientation is due to additional signal production that occurs from the enhanced contractility (resulting in increased stretching of the integrin-ligand bonds) of the cells at large values of L_0.

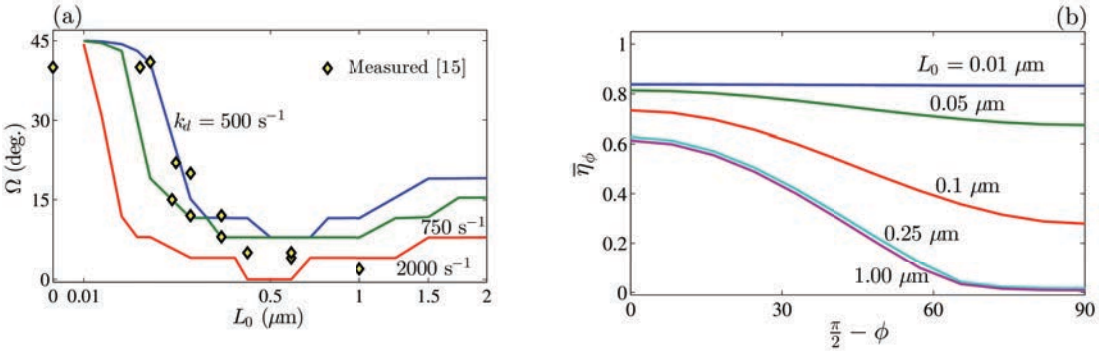

Figure 6: *(a) Comparison between the measured [16] and predicted values of the cell orientation Ω as a function of the pitch L_0 ($r = 0.5$) for four choices of the de-phosphorylation rate constant k_d. (b) Predictions of $\bar{\eta}_\phi$ as function of $\pi/2 - \phi$ for selected values of L_0 ($r = 0.5$) and the reference value of k_d.*

The predictions discussed above demonstrate the fidelity of the model in estimating the response of cells on grooved substrates. The key ingredient that enables the model to capture this behavior is that it includes a spatially inhomogeneous activation signal

that arises from the fact that Rho activation only occurs at the focal adhesion sites, i.e. only along the ridges in the case of a grooved substrate. The consequences of this are that: (i) reducing the ratio r of the width of the ridge to the groove results in a higher level of alignment of the cells with the grooves as there is insufficient signal production to allow for fibers that bridge across the grooves to form and (ii) models that use spatially uniform signals for the activation of stress fibers (e.g. Refs. [17-20]) would not only predict that the stress fiber network is spatially uniform for cells on a grooved substrate but also that the network is isotropically distributed for all values of L_0, i.e. $\Omega = 45^o \forall\, L_0$. These aspects of the model are further elucidated in the supplementary material.

4. Concluding remarks

The response of osteoblasts on grooved substrates is investigated via a model that accounts for the complex feedback between focal adhesion formation on the ridges, the triggering of signaling pathways by the formation of these adhesions and the development of the stress fiber network due to these activation signals. The distance over which signaling proteins activated at the adhesions on the ridges diffuse into the remainder of the cytosol (prior to being dephosphorylated) governs the formation of the actin network. For small groove pitches (less than about 100 nm) the signaling proteins diffuse throughout the cytosol resulting in a reasonably spatially homogenous and isotropic stress fiber network. Thus, the orientation of cells in such cases is random. By contrast, when the groove pitch is large (on the order of 1 μm) the signaling proteins de-phosphorylate before they can diffuse into the portion of the cell over the grooves. Therefore, in this case not only does the cytoskeletal network form mainly on the ridges but also the fibers are mainly aligned with the direction of the ridges (or grooves). This results in the cells orienting themselves so as to be aligned with the grooves. The model thus provides a possible explanation for the observations of Lamers et al. [16] on the basis of the spatial inhomogeneity of the activation signal for stress fibers. In particular it shows that the lower limit of the groove spacing for an interaction between the grooves and the cells is about 100 nm but the interaction is lost with cells orienting randomly on substrates with groove spacings smaller than 50 nm.

Ethics

This manuscript describes mathematical models and illustrates the results of numerical simulations, therefore no ethical considerations apply.

Data accessibility

This manuscript does not report primary experimental data. All relevant simulation parameters have been detailed in the main text and supplementary material.

Competing interests

We have no competing interests

Authors' contributions

VSD conceived the study. VSD and RMMcM devised the mathematical models. AV implemented the mathematical models and produced the numerical results. VSD wrote the paper. RMMcM and AV contributed to the revision of the paper.

Funding
AV and VSD acknowledge the Royal Society for supporting AV through a Newton International Fellowship.

References

1. Engler, A.J., S. Sen, H.L. Sweeney, and D.E. Discher, "Matrix Elasticity Directs Stem Cell Lineage Specification". Cell. **126**(4): p. 677-689, 2006.
2. Nelson, C.M., R.P. Jean, J.L. Tan, W.F. Liu, N.J. Sniadecki, A.A. Spector and C.S. Chen, "Emergent patterns of growth controlled by multicellular form and mechanics". Proceedings of the National Academy of Sciences of the United States of America. **102**(33): p. 11594-11599, 2005.
3. McBeath, R., D.M. Pirone, C.M. Nelson, K. Bhadriraju, and C.S. Chen, "Cell Shape, Cytoskeletal Tension, and RhoA Regulate Stem Cell Lineage Commitment". Developmental Cell. **6**(4): p. 483-495, 2004.
4. McMurray, R.J., N. Gadegaard, P.M. Tsimbouri, K.V. Burgess, L.E. McNamara, R. Tare, K. Murawski, E. Kingham, R.O.C. Oreffo, and M.J. Dalby, "Nanoscale surfaces for the long-term maintenance of mesenchymal stem cell phenotype and multipotency". Nature Materials. **10**(8): p. 637-644, 2011.
5. Weiner, S. and H.D. Wagner, "The material bone: Structure mechanical function relations". Annual Review of Materials Science. **28**: p. 271-298, 1998.
6. Hansen, J.C., J.Y. Lim, L.C. Xu, C.A. Siedlecki, D.T. Mauger, and H.J. Donahue, "Effect of surface nanoscale topography on elastic modulus of individual osteoblastic cells as determined by atomic force microscopy". Journal of Biomechanics. **40**(13): p. 2865-2871, 2007.
7. Lim, J.Y., J.C. Hansen, C.A. Siedlecki, R.W. Hengstebeck, J. Cheng, N. Winograd, and H.J. Donahue, "Osteoblast adhesion on poly(L-lactic acid)/polystyrene demixed thin film blends: Effect of nanotopography, surface chemistry, and wettability". Biomacromolecules. **6**(6): p. 3319-3327, 2005.
7. Dalby, M.J., D. McCloy, M. Robertson, C.D.W. Wilkinson, and R.O.C. Oreffo, "Osteoprogenitor response to defined topographies with nanoscale depths". Biomaterials. **27**(8): p. 1306-1315, 2006.
8. Guido, S. and R.T. Tranquillo, "A Methodology for the Systematic and Quantitative Study of Cell Contact Guidance in Oriented Collagen Gels - Correlation of Fibroblast Orientation and Gel Birefringence". Journal of Cell Science. **105**: p. 317-331, 1993.
9. Tranquillo, R.T., "Self-organization of tissue-equivalents: the nature and role of contact guidance". Cell Behaviour: Control and Mechanism of Motility(65): p. 27-42, 1999.
11. Foolen, J., V.S. Deshpande, F.M.W. Kanters, and F.P.T. Baaijens, "The influence of matrix integrity on stress-fiber remodeling in 3D". Biomaterials. **33**(30): p. 7508-7518, 2012.
12. Eastwood, M., V.C. Mudera, D.A. McGrouther, and R.A. Brown, "Effect of precise mechanical loading on fibroblast populated collagen lattices: Morphological changes". Cell Motility and the Cytoskeleton. **40**(1): p. 13-21, 1998.

13. Henshaw, D.R., E. Attia, M. Bhargava, and L.A. Hannafin, "Canine ACL fibroblast integrin expression and cell alignment in response to cyclic tensile strain in three-dimensional collagen gels". Journal of Orthopaedic Research. **24**(3): p. 481-490, 2006.
14. Rubbens, M.P., A. Driessen-Mol, R.A. Boerboom, M.M.J. Koppert, H.C. van Assen, B.M.T. Romeny, F.P.T. Baaijens, and C.V.C. Bouten, "Quantification of the Temporal Evolution of Collagen Orientation in Mechanically Conditioned Engineered Cardiovascular Tissues". Annals of Biomedical Engineering. **37**(7): p. 1263-1272, 2009.
15. Tan, J.L., J. Tien, D.M. Pirone, D.S. Gray, K. Bhadriraju, and C.S. Chen, "Cells lying on a bed of microneedles: An approach to isolate mechanical force". Proceedings of the National Academy of Sciences of the United States of America. **100**(4): p. 1484-1489, 2003.
16. Lamers, E., X.F. Walboomers, M. Domanski, J. te Riet, F.C.M.J.M. van Delft, R. Luttge, L.A.J.A. Winnubst, H.J.G.E. Gardeniers, and J.A. Jansen, "The influence of nanoscale grooved substrates on osteoblast behavior and extracellular matrix deposition". Biomaterials. **31**(12): p. 3307-3316, 2010.
17. Deshpande, V.S., R.M. McMeeking, and A.G. Evans, "A bio-chemo-mechanical model for cell contractility". Proceedings of the National Academy of Sciences of the United States of America. **103**(38): p. 14015-14020, 2006.
18. Obbink-Huizer, C., C.W.J. Oomens, S. Loerakker, J. Foolen, C.V.C. Bouten, and F.P.T. Baaijens, "Computational model predicts cell orientation in response to a range of mechanical stimuli". Biomechanics and Modeling in Mechanobiology. **13**(1): p. 227-236, 2014.
19. Vernerey, F.J. and M. Farsad, "A constrained mixture approach to mechano-sensing and force generation in contractile cells". Journal of the Mechanical Behavior of Biomedical Materials. **4**(8): p. 1683-1699, 2011.
20. Stalhand, J., A. Klarbring, and G.A. Holzapfel, "A mechanochemical 3D continuum model for smooth muscle contraction under finite strains". Journal of Theoretical Biology. **268**(1): p. 120-130, 2011.
21. McGarry, J.P., J. Fu, M.T. Yang, C.S. Chen, R.M. McMeeking, A.G. Evans, and V.S. Deshpande, "Simulation of the contractile response of cells on an array of micro-posts". Philosophical Transactions of the Royal Society a-Mathematical Physical and Engineering Sciences. **367**(1902): p. 3477-3497, 2009.
22. Wei, Z.S., V.S. Deshpande, R.M. McMeeking, and A.G. Evans, "Analysis and interpretation of stress fiber organization in cells subject to cyclic stretch". Journal of Biomechanical Engineering-Transactions of the Asme. **130**(3)2008.
23. Ronan, W., V.S. Deshpande, R.M. McMeeking, and J.P. McGarry, "Numerical investigation of the active role of the actin cytoskeleton in the compression resistance of cells". Journal of the Mechanical Behavior of Biomedical Materials. **14**: p. 143-157, 2012.
24. Deshpande, V.S., M. Mrksich, R.M. McMeeking, and A.G. Evans, "A bio-mechanical model for coupling cell contractility with focal adhesion formation". Journal of the Mechanics and Physics of Solids. **56**(4): p. 1484-1510, 2008.
25. Pathak, A., V.S. Deshpande, R.M. McMeeking, and A.G. Evans, "The simulation of stress fibre and focal adhesion development in cells on patterned substrates". Journal of the Royal Society Interface. **5**(22): p. 507-524, 2008.

26. Pathak, A., R.M. McMeeking, A.G. Evans, and V.S. Deshpande, "An Analysis of the Cooperative Mechano-Sensitive Feedback Between Intracellular Signaling, Focal Adhesion Development, and Stress Fiber Contractility". Journal of Applied Mechanics-Transactions of the Asme. **78**(4)2011.
27. Hill, A.V., "The Heat of Shortening and the Dynamic Constants of Muscle". Proceedings of the Royal Society of London. Series B, Biological Sciences. **126**(843): p. 136-195, 1938.
28. Lennard-Jones, J.E., "Cohesion". Proceedings of the Physical Society. **43**: p. 461-482, 1931.
29. Oakes, P.W. and M.L. Gardel, "Stressing the limits of focal adhesion mechanosensitivity". Current Opinion in Cell Biology. **30**: p. 68-73, 2014.
30. Théry, M., A. Pépin, E. Dressaire, Y. Chen and M. Bornens, "Cell distribution of stress fibres in response to the geometry of the adhesive environment". Cell motility and the cytoskeleton. **63**: p. 341-355, 2006.
31. Tanner, K., Boudreau, A., Bissell, M.J. and S. Kumar, "Dissecting Regional Variations in Stress Fiber Mechanics in Living Cells with Laser Nanosurgery". Biophysical Journal. **99**(9): p. 2775-2783, 2010.
32. Otsuji M., Ishihara S., Co C., Kaibuchi K., Mochizuki A. and S. Kuroda, " A mass conserved reaction-diffusion system captures properties of cell polarity", PLos Computational Biology. **3**(6): p. 1040-1054, 2007.
33. Lauffenburger, D.A. and J.J. Linderman, "Receptors: Models for Binding, Trafficking, and Signalling". 1996: Oxford University Press.
34. Leckband, D. and J. Israelachvili, "Intermolecular forces in biology". Quarterly Reviews of Biophysics. **34**(2): p. 105-267, 2001.
35. McCleverty, C.J. and R.C. Liddington, "Engineered allosteric mutants of the integrin alpha M beta 2 I domain: structural and functional studies". Biochemical Journal. **372**: p. 121-127, 2003.
36. Merkel, R., P. Nassoy, A. Leung, K. Ritchie, and E. Evans, "Energy landscapes of receptor-ligand bonds explored with dynamic force spectroscopy". Nature. **397**(6714): p. 50-53, 1999.
37. Kaunas, R., P. Nguyen, S. Usami, and S. Chien, "Cooperative effects of Rho and mechanical stretch on stress fiber organization". Proceedings of the National Academy of Sciences of the United States of America. **102**(44): p. 15895-15900, 2005.

Supplementary material

1. Numerical solution technique

The governing Eqs. (2.1)-(2.13) represent a coupled set of partial differential equations (PDEs) in space and time and require a complex solution methodology. Briefly, at a given time, t, the mechanical equilibrium problem and the stress fiber evolutions equations are solved in a coupled manner using a finite element spatial discretization and the solution variables at the next time increment $t + dt$ obtained via a Runga-Kutta time integration. This solution then gives the additional stretch of the integrin-ligand bonds in the time step and is used to update the focal adhesion distributions by solving the parabolic PDE, Eq. (2.10), again using a finite element scheme for the spatial discretization but an Euler-Backward scheme for time integration in order to ensure stability of the solution. With the change in the focal adhesion concentrations in time dt now available we solve the signaling Eqs. (2.1) and (2.2) again using a finite element spatial discretization and a backward Euler time integration scheme. This gives a complete solution at time $t + dt$ and the process is repeated until steady-state is attained.

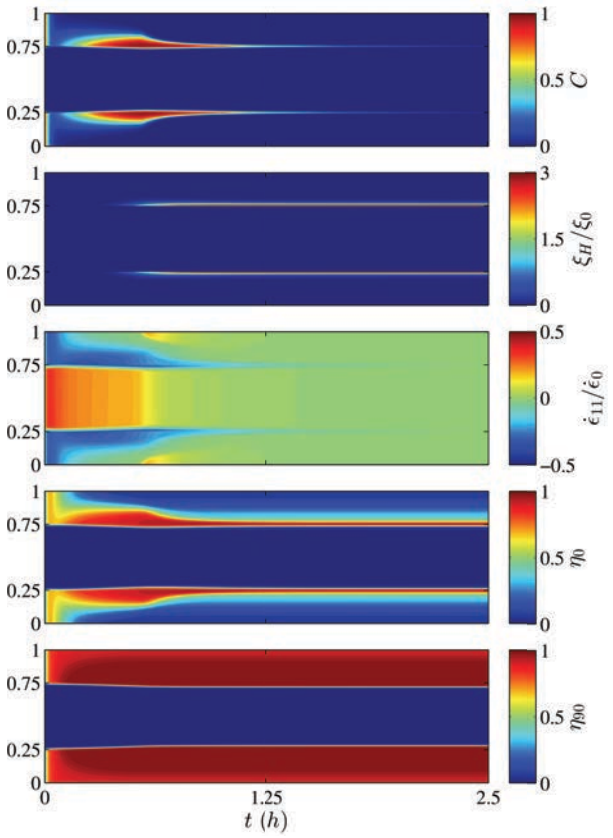

Figure S1: *Contour plots of the spatio-temporal distributions of* C, ξ_H/ξ_0, $\dot{\varepsilon}_{11}/\dot{\varepsilon}_0$ *as well as* η_0 *and* η_{90} *for cells on substrates with a pitch* $L_0 = 2\ \mu m$. *Recall that the groove spans the range* $0.25 \leq x_1/L_0 \leq 0.75$.

2. Response of cells for large groove widths

The results of Fig. 6a suggest that cells start to reorient themselves away from the groove direction for values of $L_0 > 1$ μm. In order to understand this change in the

mechanism we plot contours of the spatio-temporal evolution of C, ξ_H/ξ_0, $\dot{\varepsilon}_{11}/\dot{\varepsilon}_0$ as well as η_0 and η_{90} in Fig. S1 for the $L_0 = 2$ μm case ($r = 0.5$) analogous to the results in Fig. 4. However, here the temporal axis extends to 2.5 h instead of just 1 h as in Fig. 4. This protraction of the temporal axis is required as steady-state is now attained at approximately $t = 2.5$ h due to the additional signal generation near the edge of the ridges over the time range $0.3 \leq t \leq 2.0$ h. This additional signaling is much more significant in the $L_0 = 2$ μm case compared to the $L_0 = 1$ μm case discussed in the main body of the paper. To understand this, observe that the integrin concentrations in the $L_0 = 2$ μm case are about three orders of magnitude larger compared to the $L_0 = 1$ μm case (compare Figs. S1 and 4b). Moreover, $\xi_H/\xi_0 > 1$ near the edges of the ridges for cells on the $L_0 = 2$ μm substrates. This indicates that the additional stretching of the integrin-ligand bonds on the ridges results in a diffusive flux of integrins towards the ridge edges from the neighboring parts of the cell membrane. This large-scale adhesion formation induces high levels of C and finally higher levels of the stress fiber concentrations. This effect is evident in the steady-state spatial distributions of the stress fiber concentrations η_0 and η_{90} plotted in Fig. S2a. While the stress fiber concentrations still vanish across the central section of the cell over the groove, the distribution is less anisotropic above the ridges compared to the $L_0 = 1$ μm case. (e.g. with $L_0 = 2$ μm the distribution is isotropic at $x_1/L_0 = 0.25$). The reduction in anisotropy due to the additional signaling triggers the reorientation of the cell as parameterized by Ω in Fig. 6a.

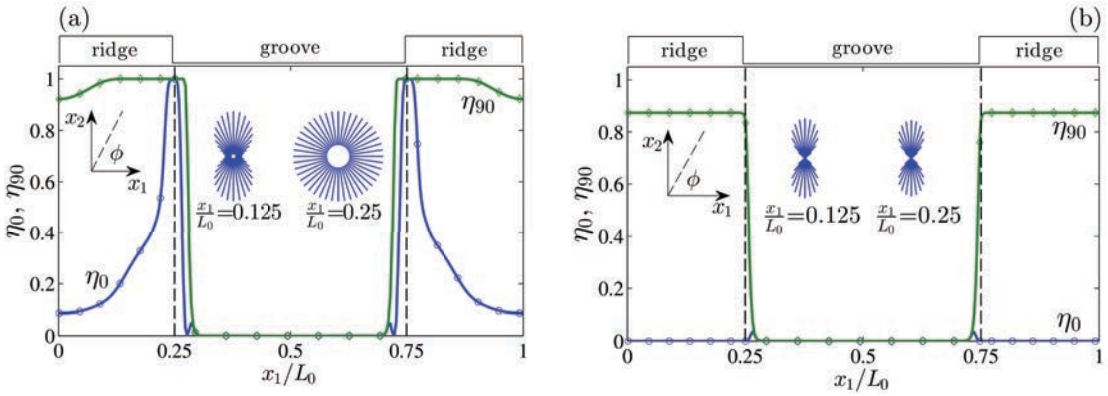

Figure S2: *The spatial distributions of the stress fiber concentrations η_0 and η_{90} at steady-state. Circular histograms of η at steady-state are included as insets at two selected locations within the cell. (a) Full model. (b) Model with the production term deleted from Eq. (2.1).*

In order to further clarify the role of this additional signaling we performed calculations with the signal production term, $(\alpha/b)\max(0, \dot{\xi}_H)$, deleted from Eq. (2.1). The remainder of the problem, including the initial and boundary conditions, remains identical to that described in Section 2. Predictions with this modification to the model of the spatio-temporal evolution of C are reported in Fig. S3 for the $L_0 = 2$ μm case ($r = 0.5$) and reference value of k_d. Comparing Figs. S1 and S2 shows that the unfolded ROCK concentration decays significantly faster when signal production due to mechano-sensitive adhesions is inhibited and thus the time scale in Fig. S2 is only $0 \leq t \leq 0.5$ h. The consequence of this reduction in the signal duration is a drop in the stress fiber concentration levels, especially in the $\phi = 0^o$ direction. To illustrate this we plot in Fig. S2b the steady-state spatial distributions of η_0 and η_{90} and the corresponding circular histograms of η

at two locations in the cell. A comparison with the corresponding distributions in Fig. S2a clearly show the increase in the anisotropy of the stress fiber distribution when the production term is deleted from Eq. (2.1).

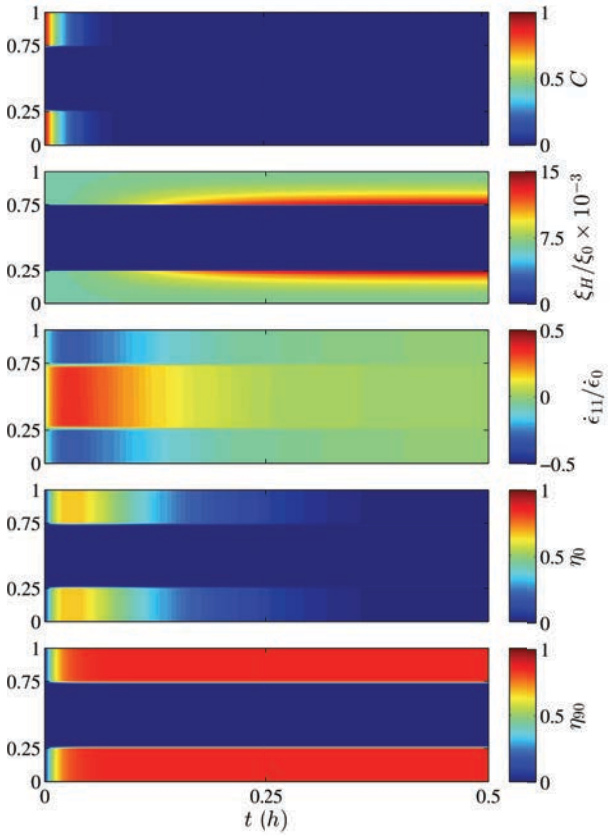

Figure S3: *Contour plots of the spatio-temporal distributions of* C, ξ_H/ξ_0, $\dot{\epsilon}_{11}/\dot{\epsilon}_0$ *as well as* η_0 *and* η_{90} *for cells on substrates with a pitch* $L_0 = 2\ \mu m$ *for the model with the production term deleted from Eq. (2.1). Recall that the groove spans the range* $0.25 \leq x_1/L_0 \leq 0.75$.

Predictions of the cell orientation Ω as a function of L_0 for the $r = 0.5$ substrates are included in Fig. S4a (dashed line) for the reference value of k_d (again using the non-linear x-axis scale, $\sqrt{L_0}$, consistent with Fig. 6a). The corresponding predictions of the full model are also reproduced in Fig. S4a from Fig. 6a. The predictions of the two models are nearly identical up to $L_0 = 1$ μm, suggesting that the additional signal production in those cases is not sufficient to affect the actin stress fiber distributions significantly. However, at larger values of L_0 the full model predicts the reorientation of the cells away from the groove direction to a more random orientation. Nevertheless, this reorientation does not occur when the production term is deleted from Eq. (2.1) with the cells continuing to further align themselves with the grooves with increasing L_0. This clearly demonstrates that it is the signal production term in Eq. (2.1) that results in change in the response of cells for $L_0 > 1$ μm.

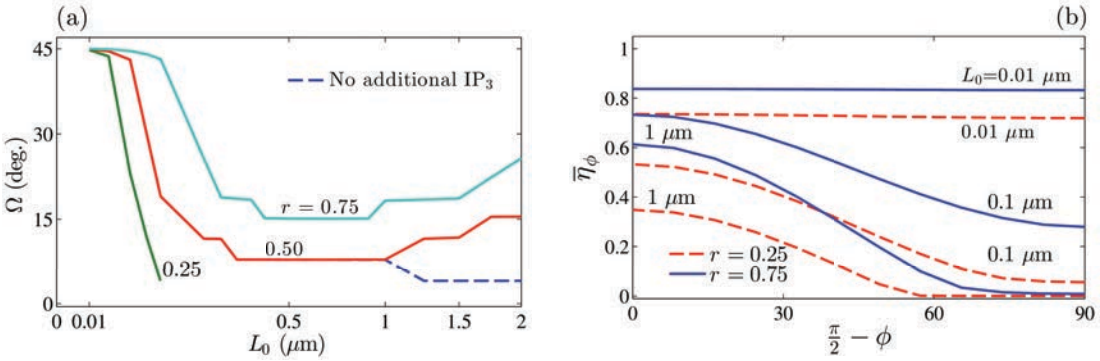

Figure S4: *(a) Predictions of the cell orientation Ω as a function of the pitch L_0 for three values the substrate ridge fraction r. Predictions are also included for the $r = 0.5$ substrate with the signal production termed in Eq. (2.1) switched-off (dashed line). (b) Predictions of $\bar{\eta}_\phi$ versus $\pi/2 - \phi$ for three selected values of L_0 for substrates with $r = 0.25$ (solid lines) and $r = 0.75$ (dashed lines) using the full model.*

Animations that illustrate the evolution of C, ξ_H/ξ_0, $\dot{\epsilon}_{11}/\dot{\epsilon}_0$, η_0 and η_{90}, as well as the circular the distribution of η at selected locations in the cell lying on the $L_0 = 2$ μm substrate ($r = 0.5$) are included with the supplementary material files. Animations with predictions of both the full model and signal production term in Eq. (2.1) deleted are also included.

There are numerous experiments of cells on patterned substrates with pitch lengths on the order of 10 μm (e.g. Tan et al. [15] reported the response of cells on a bed of posts with a spacing of 10 μm). In those experiments a strong network of stress fibers is formed between the posts though presumably the activation signals would still have been initiated only at the focal adhesions on the posts. We speculate here that the larger spacings in those experiments result in much higher levels of signals by the mechanism discussed here. This allows for stress fibers to form between the posts and provides some indirect evidence for the predictions made here that additional activation signals are generated for L_0 values typically in excess of 1 μm.

3. Effect of substrate geometry

In the experiments of Lamers et al. [16], the ratio of the ridge width to pitch was kept fixed at $r = 0.5$ and the pitch L_0 varied. Here we investigate the sensitivity of the cell orientation Ω to L_0 for two additional values of $r = 0.25$ and 0.75 and the reference value of k_a.

Predictions of $\bar{\eta}_\phi$ versus $\pi/2 - \phi$ are included in Fig. S4b for three selected values of L_0 for substrates with $r = 0.75$ (solid lines) and $r = 0.25$ (dashed lines). It is evident that for a given value of L_0 the stress fiber distributions are not only more isotropic in the $r = 0.75$ case compared to $r = 0.25$ but also the absolute concentration levels are higher for the substrate with $r = 0.75$. This is because the adhesion areas are larger for the substrate with a higher fraction of ridges and these larger adhesion areas allow larger levels of signal for the stress fibers to be generated. Predictions of the cell orientation Ω as a function of L_0 are included in Fig. S4a for the three values of $r = 0.25, 0.5$ and 0.75. Clearly with increasing r, the cell orientation remains random

(i.e. $\Omega = 45^o$) until larger values of L_0. Moreover, the model predicts a higher mean cell orientation of $\Omega \approx 20^o$ even at large values of L_0 for the $r = 0.75$ case. This, is in contrast to the observations (and to the model predictions) for the $r = 0.5$ case where cells align with the ridges with $\Omega \approx 0^o$ at large values of L_0. On the other hand, Ω decreases sharply with increasing L_0 for substrates with $r = 0.25$ and in fact for $L_0 \geq 0.1$ μm we cannot define Ω as $\bar{\eta}_\phi < 0.5 \; \forall \; \phi$. The model thus predicts that the tendency for cells to orient themselves along the grooves (or ridges) with increasing L_0 will decrease with increasing r. The fidelity of this prediction remains to be confirmed experimentally.

4. Effect of spatially inhomogeneous activation signal

The predictions of cell alignment (due to the anisotropic distributions of the stress fibers) are a consequence of the spatially inhomogeneous unfolded ROCK concentration resulting from this coupled model. Most models for cell contractility and the evolution of the stress fiber network in the literature to-date (e.g. Refs. [17-20]) have decoupled the activation signal from the focal adhesion and contractile response of cells. In these models, a spatially homogenous activation signal is imposed in terms of the parameter C in Eq. (2.3).

To understand the limitations of imposing a spatially homogenous signal we consider the case of spatially homogenous C for the problem analysed above. The governing equations are identical to those in Section 2, except for the fact that Eqs. (2.1) and (2.2) are no longer needed to calculate $0 \leq C \leq 1$ as it is directly imposed in Eq. (2.3) as a spatially uniform (but possibly temporally varying) function. The boundary conditions are also identical to those described in Section 2 but again the boundary conditions to Eq. (2.1) are no longer relevant. The steady-state solution to the governing equations is then given by $u_1 = \varepsilon_{11} = 0, \forall x_1$ and $\eta(\phi) = \eta_0, \forall x_1$, where $0 \leq \eta_0 \leq 1$ is a constant dependent on the imposed C. Moreover, with $u_1 = 0$, there is no stretching of the integrin-ligand bonds on the ridges and hence ξ_H/ξ_0 is also piecewise uniform and given by Eq. (2.15) on the ridges and by Eq. (2.14) on the portion of the cells over the grooves.

Thus, the spatially uniform signal not only predicts that the stress fiber network is spatially uniform for cells on a grooved substrate but also isotropic for all values of L_0, i.e. $\Omega = 45^o \forall \; L_0$, contrary to the observations of Lamers et al. [16]. We thus argue that the spatially inhomogeneous activation signal, with signal production occurring at the focal adhesion sites on the ridges, is critical in capturing the observed actin network and cell orientation for cells on grooved substrates.

Video Captions

Movie M1 (Movie_M1.avi): *Animation showing spatial distribution of* C, ξ_H/ξ_0, $\dot{\epsilon}_{11}/\dot{\epsilon}_0$, η_0 *and* η_{90}, *as well as the circular the distribution of* η *at selected locations over the pitch length for the* $L_0 = 0.05 \; \mu m$ *case. Note that time is scaled in the movies to be able to clearly show the early fast changes as well as the final steady-state.*

Movie M2 (Movie_M2.avi): *Animation showing spatial distribution of* C, ξ_H/ξ_0, $\dot{\epsilon}_{11}/\dot{\epsilon}_0$, η_0 *and* η_{90}, *as well as the circular the distribution of* η *at selected locations over the pitch length for the* $L_0 = 1.0\ \mu m$ *case. Note that time is scaled in the movies to be able to clearly show the early fast changes as well as the final steady-state.*

Movie M3 (Movie_M3.avi): *Animation showing spatial distribution of* C, ξ_H/ξ_0, $\dot{\epsilon}_{11}/\dot{\epsilon}_0$, η_0 *and* η_{90}, *as well as the circular the distribution of* η *at selected locations over the pitch length for the* $L_0 = 2.0\ \mu m$ *case. Note that time is scaled in the movies to be able to clearly show the early fast changes as well as the final steady-state.*

Movie M4 (Movie_M4.avi): *Animation showing spatial distribution of* C, ξ_H/ξ_0, $\dot{\epsilon}_{11}/\dot{\epsilon}_0$, η_0 *and* η_{90}, *as well as the circular the distribution of* η *at selected locations over the pitch length for the* $L_0 = 2.0\ \mu m$ *case and the production term deleted from Eq. (2.1). Note that time is scaled in the movies to be able to clearly show the early fast changes as well as the final steady-state.*